Applied Physics Letters

$GaAs/Al_{0.15}Ga_{0.85}As$ terahertz quantum cascade lasers with double-phonon resonant depopulation operating up to 172 K

Cite as: Appl. Phys. Lett. **97**, 131111 (2010); https://doi.org/10.1063/1.3496035
Submitted: 22 July 2010 . Accepted: 10 September 2010 . Published Online: 01 October 2010

Robert W. Adams, Karun Vijayraghavan, Qi Jie Wang, Jonathan Fan, Federico Capasso, Suraj P. Khanna, A. Giles Davies, Edmund H. Linfield, and Mikhail A. Belkin

GaAs/$Al_{0.15}Ga_{0.85}As$ terahertz quantum cascade lasers with double-phonon resonant depopulation operating up to 172 K

Robert W. Adams,[1] Karun Vijayraghavan,[1] Qi Jie Wang,[2] Jonathan Fan,[2] Federico Capasso,[2] Suraj P. Khanna,[3] A. Giles Davies,[3] Edmund H. Linfield,[3] and Mikhail A. Belkin[1,a)]

[1]*Department of Electrical and Computer Engineering, University of Texas at Austin, Austin, Texas 78758, USA*

[2]*School of Engineering and Applied Sciences, Harvard University, Cambridge, Massachusetts 02138, USA*

[3]*School of Electronic and Electrical Engineering, University of Leeds, Leeds LS2 9JT, United Kingdom*

(Received 22 July 2010; accepted 10 September 2010; published online 1 October 2010)

We report the design and performance of GaAs/$Al_{0.15}Ga_{0.85}As$ terahertz quantum cascade lasers with double-phonon resonant depopulation and a vertical lasing transition. Devices were processed into gold-clad double-metal waveguides. Lasing at 3 THz was observed up to a heat-sink temperature of 172 K, which compares favorably with the performance of single-phonon resonant depopulation devices based on vertical lasing transitions. These results demonstrate that terahertz quantum cascade lasers based on double-phonon depopulation designs may be a viable alternative to single-phonon depopulation designs for achieving high-temperature operation. © *2010 American Institute of Physics*. [doi:10.1063/1.3496035]

Since their initial demonstration in 2002,[1] terahertz quantum cascade lasers (THz QCLs) have developed remarkably. The maximum operating temperature of these devices in pulsed mode has been improved from 50 K in the initial report[1] to the current record of 186 K (in the absence of an external magnetic field).[2] Further improvement in the temperature-performance is required, however, to enable operation with thermoelectric coolers or, ideally, room temperature operation.

Two principal mechanisms are believed to prevent the operation of current THz QCL designs at higher temperatures: longitudinal optical (LO) phonon scattering of thermal electrons in the upper laser state and backfilling of the lower laser state by thermal electrons from the laser injector.[3] Currently, state-of-the-art GaAs/$Al_{0.15}Ga_{0.85}As$ THz QCLs use a single-phonon resonant depopulation scheme ("single-phonon" devices), where the lowest injector state is separated from the lower laser level by the LO phonon energy.[2–4] Since the LO phonon energy is 36 meV in GaAs and the electron temperature in a QCL is typically 50–100 K above the lattice temperature,[5] we expect to have 15%–20% of electrons in the injector backfill the lower laser state in devices operating at a lattice temperature of 180 K. Here we used a Boltzmann distribution for the estimate, which is a good approximation for THz QCLs which have low doping density so that the Fermi energy at 180 K is much lower than the lowest energy sub-band. This backfilling problem will become more pronounced as the operating temperature increases further.

THz QCLs that utilize double-phonon resonant depopulation of the lower laser state could effectively suppress thermal backfilling. In such double-phonon resonant depopulation devices ("double-phonon" devices),[6] the total energy separation between the lowest injector state and the lower laser level is twice the LO phonon energy. As a result, from the Boltzmann distribution, the backfilling is expected to be reduced to 3%–5% of the total number of electrons in the injector, assuming GaAs-based devices with electron temperature 230–280 K (which corresponds to a lattice temperature of 180 K). We note that, compared to single-phonon THz QCLs, double-phonon devices typically require a more sophisticated injector design with more energy levels. These devices may have a larger fraction of doped electrons residing in the injector during laser operation, which may lead to increase in parasitic absorption and reduction in the laser gain and will adversely affect temperature performance. A successful double-phonon THz QCL needs to have a simple injector design with little parasitic absorption and fast electron transport.

Two different double-phonon THz QCL designs have been previously reported, using the GaAs/$Al_{0.3}Ga_{0.7}As$ material system.[7] These devices operated at frequencies around 3 THz, and the best design achieved a maximum operating temperature of 138 K,[7] which is considerably lower than that achieved with single-phonon designs at similar emission frequencies.[4,8] However, it is difficult to draw any general conclusions from this comparison as the design space of double-phonon THz QCLs is virtually unexplored and the devices in Ref. 7 had complicated injectors susceptible to parasitic absorption. Furthermore, all high-performance single-phonon THz QCLs to date utilize GaAs/$Al_{0.15}Ga_{0.85}As$ materials. GaAs/$Al_{0.15}Ga_{0.85}As$ heterostructures have a conduction band offset of approximately 0.135 meV, which is a factor of two smaller than that in GaAs/$Al_{0.3}Ga_{0.7}As$/GaAs. A smaller conduction band offset allows for better energy level control in THz QCLs, and leads to a reduced interface roughness scattering and linewidth broadening.[9] In this work, we present results for double-phonon THz QCLs designed in the GaAs/$Al_{0.15}Ga_{0.85}As$ material system. In contrast to previously-reported double-phonon QCLs,[7] our devices demonstrate a temperature performance that is comparable to, or better than that of state-of-the-art single-phonon designs of similar emission frequency.

a)Electronic mail: mbelkin@ece.utexas.edu.

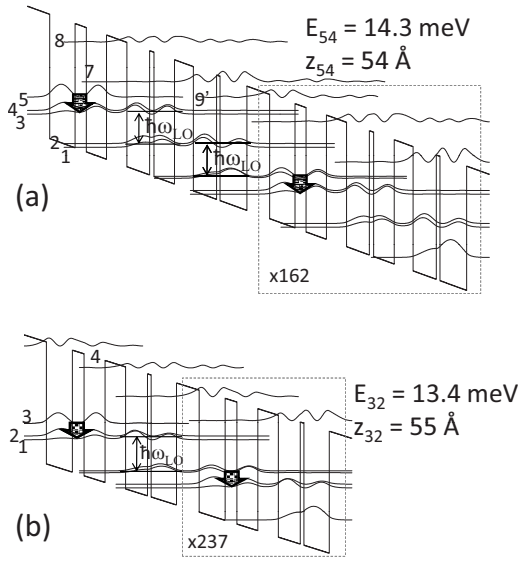

FIG. 1. Conduction band diagrams, under operating bias, of a two quantum-cascade stages of the devices with (a) double-phonon resonant depopulation and (b) single-phonon resonant depopulation active regions. A single quantum-cascade stage is marked by a dashed box and the total number of stages is indicated. The operating bias voltage was calculated to be 14.3 kV/cm and 12.8 kV/cm for double- and single-phonon devices, respectively. The layer sequences, in nanometers, for the double-phonon and single-phonon designs are, starting from the injection barrier (the barrier on the leftmost side of the band diagrams): **6.3**/7.0/**3.2**/5.6/**5.6**/6.3/**1.2**/5.7/**5.2**/6.4/**1.0**/7.4 and **6.2**/7.1/**3.2**/5.7/**5.6**/6.0/**1.0**/6.9, respectively. Here, $Al_{0.15}Ga_{0.85}As$ barriers are indicated in bold and the underlined layers are n-doped. For the double-phonon design, a 6.4 nm well was uniformly doped at 5.9×10^{16} cm^{-3}. For the single-phonon design, 2.5 and 2.4 nm sections of the 6.0 and 6.9 nm wells immediately adjacent to the 1 nm barrier were n-doped at 5×10^{16} cm^{-3}. Grey arrows indicate lasing transitions, with energies and dipole moments as indicated. Phonon transitions are indicated as ω_{LO}.

The conduction band diagram for the double-phonon devices tested in this work is shown in Fig. 1(a). For comparison, we also designed and tested single-phonon THz QCLs based on a similar design concept; the band diagram for these devices is shown in Fig. 1(b). The values of the transition dipole moments and upper-lower laser level spacing in both laser designs are also shown. To reduce current leakage from the upper laser state and parasitic absorption, we made an effort to maximize the energy separation between the electron levels needed for laser operation and parasitic levels. In particular, we used a two-well injector design to push parasitic energy levels [levels 7 and 8 in Fig. 1(a) and level 4 in Fig. 1(b)] higher in energy compared to their positions in three-quantum-well THz QCLs (Refs. 2, 4, and 10) and a possible double-phonon derivative of these devices.

Both lasers were designed with injection and extraction anticrossing energies of $\Delta_{inj}\approx2.0$ meV and $\Delta_{extr}\approx4.0$ meV, respectively. The QCL material was grown by molecular beam epitaxy on an undoped GaAs substrate; the growth sequence started with a 250-nm-thick undoped GaAs buffer layer. This was followed by a 300-nm-thick $Al_{0.5}Ga_{0.5}As$ etch-stop layer, a 75-nm-thick layer of GaAs *n*-doped to 5×10^{18} cm^{-3}, a 10-μm-thick active region consisting of multiple repetitions of the layer sequences listed in the Fig. 1 caption, and finally a 50-nm-thick GaAs layer *n*-doped to 5×10^{18} cm^{-3}. The material was processed into Ti/Au metal-metal waveguides using thermocompression wafer bonding in a process similar to that outlined in Ref. 8. The top metal cladding layer consisted of 10 nm Ti/180 nm Au, and the bottom metal cladding layer consisted of 10 nm Ti/500 nm Au.

Samples were cleaved into laser bars with approximately 2-mm-long laser cavities, and mounted with indium solder onto copper carriers for testing in a vacuum cryostat. Wire bonds were made directly to the upper cladding layer of the ridge waveguides. Testing was carried out in pulsed mode with 100 ns pulses at a 2.5 kHz repetition rate. Peak powers were measured with a calibrated helium-cooled silicon bolometer using two 2 in. off-axis parabolic mirrors as follows: one with a 5 cm focal length to collect light from the device, and the other with a 15 cm focal length to focus it onto the detector. Spectra were obtained using a Fourier-transform infrared spectrometer. The current-voltage (I-V) and output power-current (L-I) characteristics of the single-phonon and double-phonon devices are presented in Figs. 2(a) and 2(b), respectively. The laser power in the L-I curves was corrected for the collection efficiency of our experimental apparatus.

Figure 2 shows that, at low temperatures (78 K), double-phonon lasers have much lower threshold current densities than single-phonon devices. Since our double-phonon devices have considerably higher sheet density per QCL stage (3.8×10^{10} cm^{-2} versus 2.5×10^{10} cm^{-2}), and a higher average doping density (6.2×10^{15} cm^{-3} versus 5.9×10^{15} cm^{-3}), compared to their single-phonon counterparts, the observed lower threshold current density for double-phonon devices indicates suppression of parasitic current channels and a more efficient electron injection into the upper laser state. We note that single-phonon devices are susceptible to parasitic current that is produced by electron tunneling from the lower injector state to the upper injector state in the next QCL stage and subsequent LO-phonon relaxation.[2] Using this model we obtain parasitic current of 810 A/cm^2 for single-phonon devices, which is close to the experimental value. This approach, however, cannot be used to calculate parasitic current in double phonon devices because only at operational bias do energy levels align to allow electron transport through the whole QCL period. This property of double-phonon devices is likely the reason for lower

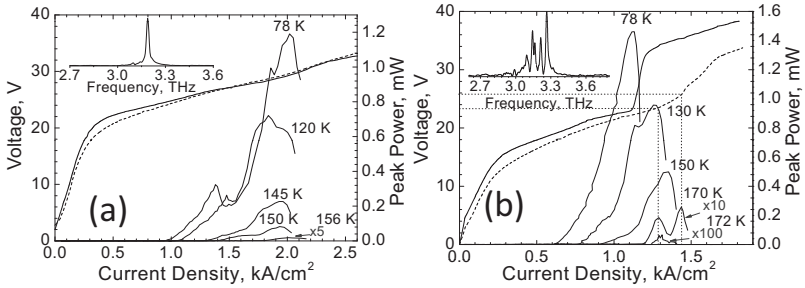

FIG. 2. Current-voltage (I-V) and light output-current (L-I) characteristics of (a) a single-phonon device, and (b) a double-phonon device, operated with 100 ns pulses at different temperatures. Solid I-V lines represent device operation at 78 K and dashed I-V lines represents device operation at 156 K for the single-phonon device and 170 K for the double-phonon device. Insets: device spectra near the peak output power at 78 K. Results were obtained with a 1.72 mm$\times$100 μm single-phonon device and a 2.3 mm$\times$120 μm double-phonon device.

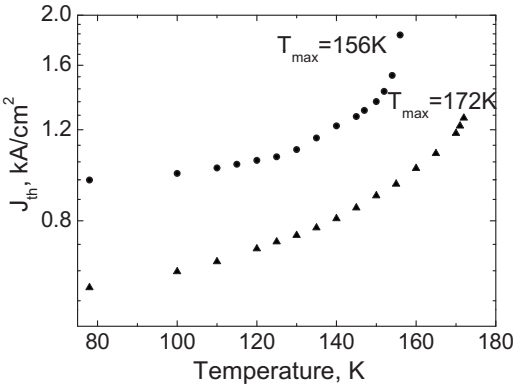

FIG. 3. Threshold current density (J_{th}) as a function of temperature for single-phonon (circles) and double-phonon (triangles) devices. Results were obtained with a 1.72 mm $\times$ 100 μm single-phonon device and a 2.3 mm $\times$ 120 μm double phonon device operated in pulsed mode with 100 ns pulses.

parasitic current. Detailed analysis of parasitic current in double-phonon devices needs to include the consideration of space-charge buildup during electron transport and is beyond the scope of this paper. The dependence of threshold current density (J_{th}) on temperature for the two device designs is shown in Fig. 3. Although the data in Fig. 3 cannot be easily fitted to obtain values of the characteristic temperature (T_0) for these devices, the plots do suggest that the double-phonon device displays a weaker temperature dependence of J_{th}.

The maximum operating temperature (T_{max}) for both device designs was achieved with devices with ridge widths of $\sim$100–120 μm. The single-phonon devices lased up to a heat sink temperature of 156 K while the double-phonon devices operated to 172 K. We note that the devices were processed with Au–Au metal waveguides, which suggests that their maximum operating temperature could be 10–15 K higher if processed into copper–copper waveguides.[4] To verify the quality of our material and processing, we also grew and processed (into Au–Au waveguides) a reference THz QCL of design similar to that reported in Ref. 4. These devices operated up to T_{max} of 164 K, which is consistent with the Ref. 4 results.

As seen in the I-V characteristics in Fig. 2, the operation voltages for both devices are considerably higher than the values of 14.3 and 12.8 V expected from the band structure calculations (Fig. 1). A similar discrepancy has been observed previously[11,12] and is likely to be due to the nonalloyed contact resistance in our structures. At higher temperatures, the L-I curve for the double-phonon device displays two peaks, with the second peak being past the onset of the "negative differential resistance" region in the I-V curve, see the L-I curve for T=170 K in Fig. 2(b). While this phenomenon is not very pronounced, it has been confirmed in all tested devices. The second peak in the L-I curve occurs at a bias voltage approximately 2.2 V above that of the initial peak. This voltage change translates into an additional 14 meV electron energy drop per quantum cascade stage which makes level 9′ aligned with the levels 3 and 4 and creates an additional current channel. We have observed that the laser emission frequency remains constant as the laser goes into the "negative differential resistance" regime and believe therefore that the effect is likely to be caused by the misalignment of electron levels "1" and "2" (Fig. 1) in the two adjacent "phonon relaxation" sections of the device band structure. In this case, most of the additional voltage drop occurs around the 5.2 nm barrier, and the region of the band structure containing the laser levels is not expected to change.

In summary, we have demonstrated high-performance THz QCLs with double-phonon resonant depopulation. Devices operated in pulsed mode up to a T_{max} of 172 K, which is the highest operating temperature achieved to date by THz QCLs with gold double-metal waveguides. Our results demonstrate that THz QCLs based on double-phonon depopulation designs are a viable alternative to single-phonon depopulation designs for achieving high-temperature operation.

The University of Texas group acknowledges support from the National Science Foundation Grant No. ECCS-0935217. Harvard University team acknowledges support from the Air Force Office of Scientific Research under Contract No. FA9550-09-1-0505-DOD. Leeds acknowledges support from the EPSRC (U.K.) EP/E048811 and both the ERC 228035-*NOTES* and 247375-*TOSCA* programs.

[1] R. Köhler, A. Tredicucci, F. Beltram, H. E. Beere, E. H. Linfield, A. G. Davies, D. A. Richie, R. C. Iotti, and F. Rossi, Nature (London) **417**, 156 (2002).
[2] S. Kumar, Q. Hu, and J. Reno, Appl. Phys. Lett. **94**, 131105 (2009).
[3] B. S. Williams, Nat. Photonics **1**, 517 (2007).
[4] M. A. Belkin, J. A. Fan, S. Hormoz, F. Capasso, S. P. Khanna, M. Lachab, A. G. Davies, and E. H. Linfield, Opt. Express **16**, 3242 (2008).
[5] M. S. Vitiello, G. Scamarcio, V. Spagnolo, B. S. Williams, S. Kumar, Q. Hu, and J. L. Reno, Appl. Phys. Lett. **86**, 111115 (2005).
[6] J. Faist, D. Hofstetter, M. Beck, T. Aellen, M. Rochat, and S. Blaser, IEEE J. Sel. Top. Quantum Electron. **38**, 533 (2002).
[7] B. S. Williams, S. Kumar, Q. Qin, Q. Hu, and J. L. Reno, Appl. Phys. Lett. **88**, 261101 (2006).
[8] B. S. Williams, S. Kumar, Q. Hu, and J. Reno, Opt. Express **13**, 3331 (2005).
[9] S. Tsujino, A. Borak, E. Müller, M. Scheinert, C. V. Falub, H. Sigg, D. Grützmacher, M. Giovannini, and J. Faist, Appl. Phys. Lett. **86**, 062113 (2005).
[10] H. Luo, S. R. Laframboise, Z. R. Wasilewski, G. C. Aers, H. C. Liu, and J. C. Cao, Appl. Phys. Lett. **90**, 041112 (2007).
[11] C. Walther, G. Scalari, J. Faist, H. Beere, and D. Ritchie, Appl. Phys. Lett. **89**, 231121 (2006).
[12] L. Lever, N. Hinchcliffe, S. P. Khanna, P. Dean, Z. Ikonic, C. A. Evans, A. G. Davies, P. Harrison, E. H. Linfield, and R. W. Kelsall, Opt. Express **17**, 19926 (2009).